Unfolding of electronic structure through induced representations of space groups: Application to Fe-based superconductors

Milan Tomić,[*] Harald O. Jeschke, and Roser Valentí

Institut für Theoretische Physik, Goethe-Universität Frankfurt, Max-von-Laue-Straße 1, 60438 Frankfurt am Main, Germany

We revisit the problem that relevant parts of band structures for a given cell choice can reflect exact or approximate higher symmetries of subsystems in the cell and can therefore be significantly simplified by an unfolding procedure that recovers the higher symmetry. We show that band-structure unfolding can be understood as projection onto induced irreducible representations of a group obtained by extending the original group of translations with a number of additional symmetry operations. The resulting framework allows us to define a generalized unfolding procedure that includes the point group operations and can be applied to any quantity in the reciprocal space. The unfolding of the Brillouin zone follows naturally from the properties of the induced irreducible representations. In this context, we also introduce a procedure to derive tight-binding models of reduced dimensionality by making use of point group symmetries. Further, we show that careful consideration of unfolding has important consequences on the interpretation of angle-resolved photoemission experiments. Finally, we apply the unfolding procedure to various representative examples of Fe-based superconductor compounds and show that the one-iron picture arises as an irreducible representation of the glide-reflection group, and we comment on the consequences for the interpretation of one-iron versus two-iron Brillouin zone representations.

　　　　PACS number(s): 71.15.Mb, 71.18.+y, 71.27.+a, 74.70.Xa

I. INTRODUCTION

Ab initio electronic structure calculations have become a primary tool of research for understanding the microscopic behavior of solids. The multitude of methods that have emerged to deal with periodic crystal systems, such as density functional theory (DFT) [1], rely on the Bloch theorem [2] in one form or another. The Bloch theorem builds upon the translational symmetry of the crystal lattice and paves the way for the fundamental concepts needed to understand the electronic structure of periodic systems, such as the classification of electronic states in terms of wave vectors $\boldsymbol{k}$ and the notion of band structure. Many important properties of the crystal, such as magnetic or transport properties, are encoded in the band structure. In addition, the band structure is important for the interpretation of a few experimental measurements such as angle-resolved photoemission spectroscopy (ARPES).

However, a problem arises in the practical use of DFT calculations whenever we have to deal with systems in which the original translational symmetry is broken. These situations are encountered, for example, in calculations on doped materials or in magnetically ordered systems. Often in these situations we have to employ large supercells whose size determines the periodicity of the band structure through the Bloch theorem. This results in a complicated band structure consisting of many bands, which is hard to interpret.

Recently, a number of methods have emerged [3–10] to alleviate this problem. A common approach shared among these methods, implicitly or explicitly, is a transformation from one Bloch basis to another.

An important aspect of the Bloch theorem is that it is an expression of one of the fundamental group-theoretical principles, which states that the eigenstates of a physical system can be classified according to the irreducible representations of its group of symmetries [11]. In light of this, the band-structure unfolding can be viewed as a transformation between the irreducible representations of different translation groups. Despite the number of recent publications [3–9], a rigorous consideration of the group-theoretical aspects of the band-structure unfolding is still missing, and as a consequence certain important properties are overlooked, especially in relation to ARPES experiments.

The purpose of this work is to attempt to close this conceptual gap by introducing a band-structure unfolding based on group theory. This treatment allows us to incorporate point group symmetries into a unified framework, and it generalizes the idea of using glide-reflection operations, initially proposed in the context of LaFeAsO [12], in order to obtain models of reduced dimensionality. Our band-structure unfolding also allows for a clear understanding of the two-Fe versus one-Fe description of the electronic properties of Fe-based superconductors.

We will show that band-structure unfolding can be achieved by projecting the bands onto the induced irreducible representations of the supergroup of the initial group of translations. We will also show that this leads naturally to the concept of the unfolded Brillouin zone. With the help of the point group operations, band structures can be unfolded beyond the limits of translational symmetry. Furthermore, tight-binding models with a reduced number of orbitals can be formulated under certain conditions.

The group-theoretical formulation of the unfolding procedure in terms of projections onto the irreducible subspaces allows us to unfold any quantity in reciprocal space if we know how it behaves under the symmetry operations of the crystal lattice. In addition, unfolding artifacts such as "ghost bands" [6] or "incomplete bands" [13] are naturally explained as bands with projections onto the multiple irreducible subspaces in cases with broken symmetry.

---

*tomic@itp.uni-frankfurt.de

II. METHOD

A. Group of translations

One of the fundamental statements in solid-state physics is that the eigenstates of the Hamiltonian of a periodic system can be classified according to the irreducible representations of the group of translational symmetries of the system. Let us denote the crystal lattice as $\mathcal{L} = \{\boldsymbol{R_n} = \sum_{i=1}^{3} n_i \boldsymbol{a_i} | n_i = 1, \ldots, N_i\}$, where $\boldsymbol{n} = (n_1, n_2, n_3)$, $N = N_1 N_2 N_3$ is the number of unit cells in the lattice, $\boldsymbol{R_n}$ are their position vectors, and $\boldsymbol{a_i}$ are the vectors spanning the unit cell. We would like to point out that the following discussion applies equally in one and two dimensions, and that we choose three dimensions for the sake of definiteness. The lattice is invariant under the action of the group of translation operators $\mathbb{T} = \{\hat{T}_{\boldsymbol{n}}\}$, such that $\boldsymbol{R_n} + \boldsymbol{R_m} = \hat{T}_{\boldsymbol{m}} \boldsymbol{R_n}$, where periodic boundary conditions $\hat{T}_{N_i} = 1$ are assumed. The translation group $\mathbb{T}$ is an Abelian cyclic group generated by the three generators $\hat{T}_{\boldsymbol{a_i}}$. As such, its irreducible representations are one-dimensional and given by $\Delta^{(\boldsymbol{k})}(\hat{T}_{\boldsymbol{n}}) = \exp(-i\boldsymbol{k} \cdot \boldsymbol{R_n})$. There are N inequivalent irreducible representations of $\mathbb{T}$ and they can be enumerated by the vector index $\boldsymbol{k} \in \mathcal{B}(\mathcal{L})$, where $\mathcal{B}(\mathcal{L}) = \{\sum_{i=1}^{3} g_i \boldsymbol{b_i} | g_i \in [0,1)\}$ is the Brillouin zone (BZ), and $\boldsymbol{b_i} = 2\pi \varepsilon_{ijk} \boldsymbol{a_j} \times \boldsymbol{a_k} / [\boldsymbol{a_1} \cdot (\boldsymbol{a_2} \times \boldsymbol{a_3})]$ are unit vectors of the reciprocal lattice $\mathcal{L}^{-1}$. To each irreducible representation $\Delta^{(\boldsymbol{k})}$ corresponds a one-dimensional subspace $\mathbb{V}_{\boldsymbol{k}}$, defined as a codomain of the projection operator

$$\hat{P}_{\boldsymbol{k}} = \frac{1}{\sqrt{N}} \sum_{\boldsymbol{n}} [\Delta^{(\boldsymbol{k})}(\hat{T}_{\boldsymbol{n}})]^\dagger \hat{T}_{\boldsymbol{n}} = \frac{1}{\sqrt{N}} \sum_{\boldsymbol{n}} \exp(i\boldsymbol{k} \cdot \boldsymbol{R_n}) \hat{T}_{\boldsymbol{n}}. \tag{1}$$

Because for all $\boldsymbol{n}$, $[\hat{T}_{\boldsymbol{n}}, \hat{H}] = 0$, the subspaces $\mathbb{V}_{\boldsymbol{k}}$ will be orthogonal irreducible subspaces of the Hamiltonian $\hat{H}$, and thus a symmetry classification of the eigenstates of the Hamiltonian is achieved.

To proceed, we assume that we have P localized electronic states, $|0, \mu\rangle$, $\mu = 1, \ldots, P$, centered at positions $\boldsymbol{s}_\mu$, occupying the unit cell located at origin $\boldsymbol{0}$. The sites $\boldsymbol{s}_\mu$ do not necessarily have to be different since we can consider cases with multiple orbitals per atomic site. The translationally invariant electronic states of the crystal lattice are obtained by the action of $\mathbb{T}$ onto these states, and the resulting localized electronic states are $|\boldsymbol{R_n}, \mu\rangle = \hat{T}_{\boldsymbol{n}} |0, \mu\rangle$ at positions $\boldsymbol{R_n} + \boldsymbol{s}_\mu$. Application of the projector (1) to the states $|0, \mu\rangle$ results in the familiar Bloch states,

$$|\boldsymbol{k}, \mu\rangle = \frac{1}{\sqrt{N}} \sum_{\boldsymbol{n}} \exp(i\boldsymbol{k} \cdot \boldsymbol{R_n}) |\boldsymbol{R_n}, \mu\rangle. \tag{2}$$

Using (2) as a basis, the Hamiltonian $\hat{H}$ is brought to the block-diagonal form, with N blocks of size $P \times P$, whose elements are given by $[\hat{H}_{\boldsymbol{k}}]_{\mu\nu} = \langle \boldsymbol{k}, \mu | \hat{H} | \boldsymbol{k}, \nu \rangle$. Every block $\hat{H}_{\boldsymbol{k}}$ can be diagonalized separately, yielding a set of P bands at $\boldsymbol{k}$. A set of bands for every $\boldsymbol{k} \in \mathcal{B}(\mathcal{L})$ represents the band structure for the given lattice $\mathcal{L}$.

B. Extension to additional symmetry operations

In many applications, the translation group $\mathbb{T}$ can be expanded with a certain number of operations, which are, approximately, symmetry operations of the lattice $\mathcal{L}$. When

this is the case, we will have a new group $\mathbb{S}$, such that $\mathbb{T}$ is an invariant subgroup of $\mathbb{S}$, denoted $\mathbb{T} \lhd \mathbb{S}$. Due to this fact, irreducible representations of $\mathbb{S}$ can be induced from $\mathbb{T}$ in a simple manner. Furthermore, the addition of every new symmetry operation will halve the number of independent states $|\boldsymbol{k}, \mu\rangle$ at every $\boldsymbol{k}$, since additional operations will produce one-half of the states $|\boldsymbol{k}, \mu\rangle$ from another half, and thus will halve the number of bands, producing the *unfolded* band structure. This is subject to certain conditions that will be outlined in the discussion that follows.

Let us assume now that we are expanding $\mathbb{T}$ with K operations $\hat{C}_i$, denoted in Seitz notation [14,15] as $\hat{C}_i = (\hat{U}_i | \boldsymbol{\tau}_i)$, $i = 1, \ldots, K$, where $\hat{U}_i$ is a point group operation and $\boldsymbol{\tau}_i$ is a fractional translation (with respect to the translations $\hat{T}_{\boldsymbol{n}}$ of $\mathbb{T}$) so that the combination of $\hat{C}_i$ and $\hat{T}_{\boldsymbol{n}}$ leads to a space group $\mathbb{S}$. Operations $\hat{C}_i$ are allowed to be pure translations but not pure point group operations, since in the case of the pure point group operations, we would not be able to interpret the unfolded band structure in terms of a lattice of reduced periodicity.

The action of $\hat{C}_i$ on an arbitrary point in the Cartesian space is given by

$$\hat{C}_i \boldsymbol{r} = \hat{U}_i \boldsymbol{r} + \boldsymbol{\tau}_i$$

while the combined action of $\hat{C}_i$ and $\hat{T}_{\boldsymbol{n}}$ results in the space group operation $\hat{S}_{\boldsymbol{n}i}$ defined as

$$\hat{S}_{\boldsymbol{n}i} \boldsymbol{r} = \hat{T}_{\boldsymbol{n}} \hat{C}_i \boldsymbol{r} = \hat{U}_i \boldsymbol{r} + \boldsymbol{R_n} + \boldsymbol{\tau}_i = (\hat{U}_i | \boldsymbol{R_n} + \boldsymbol{\tau}_i) \boldsymbol{r}.$$

The space group operators $\hat{S}_{\boldsymbol{n}i}$ induce an action on the localized states. Under the point group operations $\hat{U}_i$ and fractional translations $\boldsymbol{\tau}_i$ states, $|\boldsymbol{R_n}, \mu\rangle$ transform into each other as $(\hat{U}_i | \boldsymbol{\tau}_i) |\boldsymbol{R_n}, \mu\rangle = \sum_\nu |\boldsymbol{R_n}, \nu\rangle W_{\nu\mu}(\hat{C}_i)$, where the matrices $\hat{W}(\hat{C}_i)$ represent the action of the operations $\hat{C}_i = (\hat{U}_i | \boldsymbol{\tau}_i)$ in the basis composed of the states $|\boldsymbol{R_n}, \mu\rangle$. Their matrix elements can be written as $W_{\gamma\delta}(\hat{C}_i) = r_{\gamma\delta} \delta(\boldsymbol{s}_\delta - \hat{C}_i \boldsymbol{s}_\gamma)$, where δ is the Kronecker delta and sites $\boldsymbol{s}_\delta$ and $\hat{C}_i \boldsymbol{s}_\gamma$ are considered equal if they differ by a lattice vector. The total action of $\hat{S}_{\boldsymbol{n}i}$ is

$$\hat{S}_{\boldsymbol{n}i} |\boldsymbol{R_m}, \mu\rangle = \sum_\nu |\boldsymbol{R_m} + \boldsymbol{R_n}, \nu\rangle W_{\nu\mu}(\hat{C}_i). \tag{3}$$

The task is now to induce the irreducible representations of the space group $\mathbb{S}$. We first note that the operators $\hat{C}_i$ are the right coset representatives of $\mathbb{S}$ with respect to $\mathbb{T}$. Let the factor group, corresponding to this right coset decomposition, be $\mathbb{C} = \mathbb{S} : \mathbb{T}$. The well-known property of space groups is that every space group is solvable, that is, every space group can be decomposed into a series $\mathbb{S}_0 \lhd \mathbb{S}_1 \lhd \cdots \lhd \mathbb{S}_D = \mathbb{S}$, where every factor group in the decomposition is Abelian. In addition to that, it is always possible to find the decomposition series where the factor groups $\mathbb{C}_i = \mathbb{S}_{i+1} : \mathbb{S}_i$ are cyclic groups of index 2 or 3. This simplifies the induction procedure further, since in case the factor group $\mathbb{C}$ is not a cyclic group, we can always decompose it into a subgroup series $\mathbb{C}_0 \lhd \mathbb{C}_1 \lhd \cdots \lhd \mathbb{C}_B = \mathbb{C}$, where every $\mathbb{C}_i$ is a cyclic group.

In the induction procedure, from every irreducible representation of $\mathbb{T}$, multiple irreducible representations of $\mathbb{S}$ can be induced. Some of these irreducible representations will be one-dimensional, while some will be multidimensional. The multidimensional induced irreducible representations of $\mathbb{S}$ will

mix irreducible representations of $\mathbb{T}$ with different $\mathbf{k}$. Since our goal is to perform the unfolding within the same $\mathbf{k}$, we have to restrict ourselves only to the cases in which the induction procedure yields one-dimensional irreducible representations of $\mathbb{S}$.

C. One-dimensional irreducible representations of $\mathbb{S}$: Unfolding procedure

For every irreducible representation $\Delta^{(\mathbf{k})}$ of $\mathbb{T}$, irreducible representations of $\mathbb{S}$ are determined from the little cogroup $\mathbb{L}_{\mathbf{k}}$ [14,15]. The little cogroup is a group of all point group operations $\hat{U}_i^{\mathbf{k}}$ such that $\hat{U}_i^{\mathbf{k}} \mathbf{k} = \mathbf{k} + \mathbf{K}$, where $\mathbf{K}$ is a reciprocal-lattice vector. Given an irreducible representation $\Lambda^{(\mathbf{k},\alpha)}$ of $\mathbb{L}_{\mathbf{k}}$, an irreducible representation $\Delta^{(\mathbf{k},\alpha)}$ of $\mathbb{S}$ is induced, where the coset representatives $\hat{C}_i$ are represented by

$$\Delta^{(\mathbf{k},\alpha)}((\hat{U}_i|\boldsymbol{\tau}_i)) = \exp(-i\mathbf{k} \cdot \boldsymbol{\tau}_i)\Lambda^{(\mathbf{k},\alpha)}(\hat{U}_i)$$

and the index α runs over all irreducible representations of the little cogroup. This holds across the entire interior of the BZ, with the exception of the BZ boundary for the cases of the symmorphic space groups, where the induction procedure is more complex, and more sophisticated methods, such as Herring's method, are needed [14,15]. We will just assume that $\mathbf{k}$ never lies on the BZ boundary, but it can be arbitrarily close to it. In cases in which $\hat{U}_i = 1$, i.e., where the operators $\hat{C}_i$ are just fractional translations, which is the case of translational unfolding, the little cogroup $\mathbb{L}_{\mathbf{k}}$ will contain all fractional translations and will be the same for every $\mathbf{k}$. In this case, the irreducible representations of the little cogroup, $\Lambda^{(\mathbf{k},\alpha)}$, are taken to be the irreducible representations of the group of fractional translations, modulo $\mathbb{T}$, meaning that two fractional translations are considered to be identical if they differ by $\mathbf{R}_{\mathbf{n}}$.

When $\mathbf{k}$ is invariant (up to the reciprocal-lattice vector $\mathbf{K}$) under all point group operators of $\mathbb{C}$, then from the irreducible representation $\Delta^{(\mathbf{k})}$ of $\mathbb{T}$, K one-dimensional irreducible representations $\Delta^{(\mathbf{k},\alpha)}$ will be induced. When this is the case, the $\Lambda^{(\mathbf{k},\alpha)}(\hat{U}_i)$ will be roots of unity so that we can write, in general,

$$\Delta^{(\mathbf{k},\alpha)}((\hat{U}_i|\boldsymbol{\tau}_i)) = \exp\left(-2 f_i^{\alpha}/K\right)\exp(-i\mathbf{k} \cdot \boldsymbol{\tau}_i), \quad (4)$$

where f_i^{α} is an integer such that $0 \leqslant f_i^{\alpha} < K$. The integers f_i^{α}, with the operation of addition modulo K, constitute a group isomorphic to $\mathbb{L}_{\mathbf{k}}$. We use the convention that $\alpha = 0$ denotes the unit irreducible representation, thus $f_i^0 = 0$. When (4) is taken into account, the projectors onto the irreducible subspaces are given by

$$\hat{P}_{\mathbf{k}\alpha} = \frac{1}{\sqrt{KN}} \sum_{\mathbf{n}} \sum_{i} \exp(i\mathbf{k} \cdot \mathbf{R}_{\mathbf{n}})[\Delta^{(\mathbf{k},\alpha)}(\hat{C}_i)]^{\dagger} \hat{S}_{\mathbf{n}i}$$

so that the Bloch basis (2) corresponding to $\mathbb{S}$ can be written, in analogy to (1), as

$$|\mathbf{k},\mu,\alpha\rangle = \frac{1}{\sqrt{KN}} \sum_{\mathbf{n}} \sum_{i} \sum_{\nu} \exp\left(2\pi i f_i^{\alpha}/K\right)$$
$$\times \exp[i\mathbf{k} \cdot (\mathbf{R}_{\mathbf{n}} + \boldsymbol{\tau}_i)]|\mathbf{R}_{\mathbf{n}},\nu\rangle W_{\nu\mu}(\hat{C}_i). \quad (5)$$

By employing the basis Eq. (5), $\hat{H}_{\mathbf{k}}$ can be brought into block-diagonal form with K blocks $\hat{H}_{\mathbf{k}\alpha}$ of size $P/K \times P/K$.
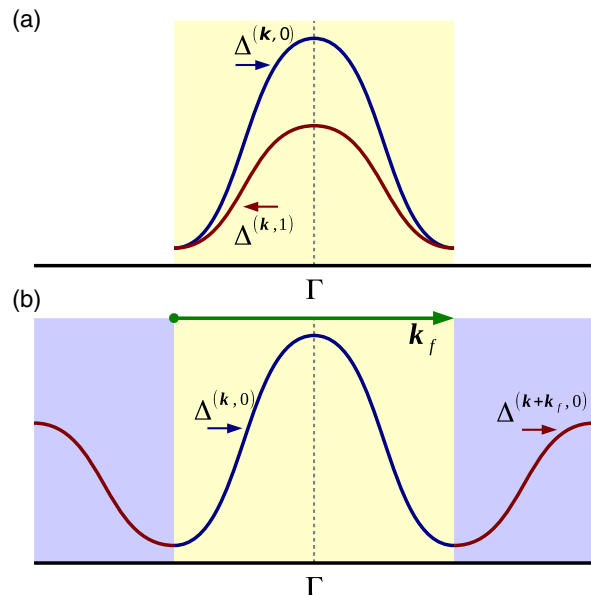

FIG. 1. (Color online) Brillouin zone unfolding. (a) Folded band structure showing two bands belonging to two irreducible representations $\Delta^{(\mathbf{k},0)}$ and $\Delta^{(\mathbf{k},1)}$ of $\mathbb{S}$. (b) The unfolded band structure shows that $\Delta^{(\mathbf{k},1)} = \Delta^{(\mathbf{k}+\mathbf{k}_f,0)}$, leading to the unfolded Brillouin zone, shown in yellow and purple backgrounds. The folding vector $\mathbf{k}_f$ is shown in green.

Each block $\hat{H}_{\mathbf{k}\alpha}$ can be diagonalized separately and will yield P/K bands. It is important to note that because of the addition of a fractional translation in Eq. (5), the reciprocal space period of blocks $\hat{H}_{\mathbf{k}\alpha}$ is larger than the BZ. Since the only difference between the blocks $\hat{H}_{\mathbf{k}\alpha}$ is in the exponential prefactor $\exp(-2\pi i f_i^{\alpha}/K)$ in Eq. (5), we can restrict ourselves to only one block, i.e., $\hat{H}_{\mathbf{k}\alpha}$, and then reproduce the other blocks by allowing $\mathbf{k}$ to leave the BZ, because we can choose $\mathbf{k}_f^{\alpha\beta} \in \mathcal{B}(\mathcal{L})$ such that

$$\mathbf{k}_f^{\alpha\beta} \cdot \mathbf{R}_{\mathbf{n}} = 2\pi z,$$
$$\mathbf{k}_f^{\alpha\beta} \cdot \boldsymbol{\tau}_i = 2\pi \frac{f_i^{\beta} - f_i^{\alpha}}{K}, \quad (6)$$

where z is an integer. In this way, we can have $\hat{H}_{\mathbf{k}\beta} = \hat{H}_{\mathbf{k}+\mathbf{k}_f^{\alpha\beta},\alpha}$. The vectors $\mathbf{k}_f^{\alpha\beta}$ are the *folding* vectors. The diagonalization of the block $\hat{H}_{\mathbf{k}\alpha}$ and its extensions outside of the BZ, by the folding vectors, produces the *unfolded* bands. The BZ, enlarged by the K folding vectors $\mathbf{k}_f^{\alpha\beta}$, is the unfolded BZ (Fig. 1).

It is important to stress here that because $\hat{C}_i$ involves the fractional translations $\boldsymbol{\tau}_i$, and due to the requirement of the one-dimensionality of the irreducible representations of $\mathbb{S}$, the unfolded band structure represents the band structure of the crystal lattice with the unit cell size reduced by a factor of K, which can be simply translationally folded back along the folding vectors to represent the starting band structure, regardless of the point group operations $\hat{U}_i$. Because of this, we can effectively describe the electronic structure with a Hamiltonian of smaller dimensionality. We can also understand this in a different way. Since $|\mathbf{k},\mu,\alpha\rangle$ are the

symmetry adapted basis vectors, no interaction contained in the Hamiltonian can cause a transition between the states with different α, thereafter all dynamical processes are contained within their respective irreducible subspaces. We have seen that different irreducible representations become equivalent if shifted by the folding vectors, meaning that no information is lost if we just keep a single irreducible representation, as long as we expand it onto the entire unfolded Brillouin zone.

One more important issue to note is that our requirement for the one-dimensional irreducible representations of $\mathbb{S}$ implies that the unfolding that utilizes the point group operations is exact only for $\mathbf{k}$ values that are invariant under all point group operations $\hat{U}_i$. For example, if we use the screw-axis operations, the unfolding will be exact only along a corresponding high-symmetry line in the Brillouin zone. However, if the electronic properties are dominantly one-dimensional along the given high-symmetry line, the unfolding can still be used across the entire Brillouin zone while preserving the accuracy up to a significant degree.

To unfold the band structure given in the Bloch basis (2), we just need to calculate the matrix elements of the projectors $\hat{P}_{k\alpha}$. The matrix elements are given by

$$[\hat{P}_{k\alpha}]_{\gamma\delta} = \langle \mathbf{k}, \gamma | \hat{P}_{k\alpha} | \mathbf{k}, \delta \rangle$$
$$= \frac{1}{K} \sum_i \exp\left(2\pi i \alpha f_i^\alpha / K\right) \exp(i\mathbf{k} \cdot \boldsymbol{\tau}_i) W_{\gamma\delta}(\hat{C}_i). \quad (7)$$

If we assume that from the band-structure calculations we obtain bands $|\mathbf{k}, n\rangle$, where n is the band index, we can unfold the bands by applying the projectors (7) to the column vector containing the projections of bands onto the localized states $w_{k,n}^\mu = \langle \mathbf{0}, \mu | \mathbf{k}, n \rangle$. In our particular case, we have used the Vienna Ab-Initio Simulations Package (VASP) [16] to obtain the band structure. Since, within the VASP package, the exponential factors $\exp(-i\mathbf{k} \cdot \mathbf{s}_\mu)$ for fractional site vector $\mathbf{s}_\mu$ are already included in the projections $w_{k,n}^\mu$, the exponential factors in Eq. (7) can be omitted, simplifying the expressions even further.

D. Unfolding of tight-binding models

In general, any observable $\hat{A}_k$ can be unfolded by employing the projectors $\hat{P}_{k\alpha}$ so that $\hat{A}_{k\alpha} = \hat{P}_{k\alpha} \hat{A}_k \hat{P}_{k\alpha}$. With the help of Eq. (5) it is also possible to unfold tight-binding models. The matrix elements of the Hamiltonian in the tight-binding model are defined in the Bloch basis Eq. (2) as

$$[\hat{H}_k]_{\mu\nu} = \langle \mathbf{0}, \mu | \hat{H} \hat{P}_k | \mathbf{0}, \nu \rangle$$
$$= \sum_{\mathbf{R}_n} t_{\mu\nu}(\mathbf{R}_n) \exp(i\mathbf{k} \cdot \mathbf{R}_n), \quad (8)$$

where $t_{\mu\nu}(\mathbf{R}_n) = \langle \mathbf{0}, \mu | \hat{H} | \mathbf{R}_n, \nu \rangle$ are the hopping energies. This result follows from $\hat{H}_k = \hat{P}_k \hat{H} \hat{P}_k$ and the fact that $\hat{H}$ commutes with $\hat{P}_k$ and that $\hat{P}_k$ is idempotent. We define the matrix composed of the hopping energies $t_{\mu\nu}(\mathbf{R}_n)$ as $\hat{t}(\mathbf{R}_n)$. The unfolding of the tight-binding model is achieved by calculating the matrix elements of the Hamiltonian in the basis Eq. (5) and then casting the resulting expression in the form

of Eq. (8),

$$[\hat{H}_{k\alpha}]_{\mu\nu} = \langle \mathbf{0}, \mu | \hat{H} \hat{P}_{k\alpha} | \mathbf{0}, \nu \rangle$$
$$= \sum_n \sum_i t_{\mu\nu}^\alpha(\mathbf{R}_n + \boldsymbol{\tau}_i) \exp[i\mathbf{k} \cdot (\mathbf{R}_n + \boldsymbol{\tau}_i)], \quad (9)$$

where the corresponding hopping energy matrix is $\hat{t}^\alpha(\mathbf{R}_n + \boldsymbol{\tau}_i)$. The hopping energies of the unfolded TB model can then be read off as coefficients of the exponential terms $\exp[i\mathbf{k} \cdot (\mathbf{R}_n + \boldsymbol{\tau}_i)]$. The hopping energy matrices $\hat{t}^\alpha(\mathbf{R}_n + \boldsymbol{\tau}_i)$ will have the same block-diagonal structure of $\hat{H}_{k\alpha}$. The general expression for the hopping energies is then

$$\hat{t}^\alpha(\mathbf{R}_n + \boldsymbol{\tau}_i) = \frac{\exp\left(2\pi i f_i^\alpha / K\right)}{K} \hat{t}(\mathbf{R}_n) \hat{W}(\hat{C}_i). \quad (10)$$

It should be noted here that for $K > 2$, the unfolded hopping energies can become complex due to the prefactor $\exp(2\pi i f_i^\alpha / K)$. However, this prefactor does not affect the eigenvalues and eigenvectors of $\hat{H}_{k\alpha}$ since it amounts to an overall, $\mathbf{k}$-independent, unitary transformation of the Hamiltonian. Furthermore, in the unfolded picture, we extend a single irreducible representation beyond the BZ boundaries, so that in the tight-binding model we expect to have a single set of hopping energies independent of the irreducible representation. This manifestly does not hold for Eq. (10) since the exponential prefactor depends on α. Because of this, the exponential prefactor in Eq. (10) can be dropped and the irreducible representation-independent unfolded hopping energies can be defined as

$$\hat{t}(\mathbf{R}_n + \boldsymbol{\tau}_i) = \frac{1}{K} \hat{t}(\mathbf{R}_n) \hat{W}(\hat{C}_i). \quad (11)$$

When the unfolded hopping energies are defined in this way, the index α can be omitted from Eq. (9). Since we already concluded that the $\hat{t}^\alpha(\mathbf{R}_n + \boldsymbol{\tau}_i)$ are block-diagonal, a reduction of the dimensionality of the tight-binding model is achieved. Practically, this means that orbital indices μ and ν can be taken to run only over the first block in the block-diagonalized Hamiltonian, since other blocks are symmetrically equivalent.

E. Relation to ARPES

Angle-resolved photoemission is one of the most direct ways to experimentally observe the band structure in solids [17]. However, the interpretation of raw experimental data is a very complicated process and often relies heavily on comparisons with density functional theory calculations. This becomes especially difficult in systems with broken translational symmetry, since, on the one hand, supercell calculations have to be employed by density functional theory resulting in complicated folded band structures, while on the other hand ARPES data often show the unfolded band structure, sometimes offset away from the first Brillouin zone [6,18]. This was already discussed in the context of band-structure unfolding [6]. However, some important issues were not considered, such as the fact that multiple irreducible representations are involved in the unfolding as well as the effect of high-symmetry regions of the Brillouin zone.

The observed photoelectron intensity at energy ω in ARPES experiments can be directly related to the one-electron spectral

function [19,20]

$$I(\omega) \sim \sum_{\boldsymbol{k}} \sum_{f} \sum_{ij} M_{\boldsymbol{k}fi} A_{\boldsymbol{k}ij}(\omega) M_{\boldsymbol{k}jf},$$

where $M_{\boldsymbol{k}fi} = \langle \boldsymbol{k}, f | \boldsymbol{\varepsilon} \cdot \hat{\boldsymbol{x}} | \boldsymbol{k}, i \rangle$ are the dipole matrix elements between the initial Bloch state $|\boldsymbol{k}, i\rangle$ and the final Bloch state $|\boldsymbol{k}, f\rangle$, and $\hat{A}_{\boldsymbol{k}ij}(\omega)$ are the matrix elements of the one-electron spectral function. Using the projectors from Eq. (1), this can be rewritten as

$$I(\omega) \sim \mathrm{tr}\left(\sum_{\boldsymbol{k}} \boldsymbol{\varepsilon} \cdot \hat{\boldsymbol{x}} \hat{P}_{\boldsymbol{k}} \hat{A}(\omega) \hat{P}_{\boldsymbol{k}} \boldsymbol{\varepsilon} \cdot \hat{\boldsymbol{x}} \right), \qquad (12)$$

where the trace is taken only over the final states, and $\hat{A}$ is restricted to the occupied subspace. If the observed system has approximate symmetry given by a group $\mathbb{S} \rhd \mathbb{T}$, either because (i) we have a slight breaking of the translational symmetry, or (ii) most of the contribution to the sum over $\boldsymbol{k}$ in Eq. (12) comes from the surface states lying in the high-symmetry region of the Brillouin zone, we can extend the summation over $\boldsymbol{k}$ onto the irreducible subspaces of $\mathbb{S}$ so that we have

$$I(\omega) \sim \mathrm{tr}\left(\sum_{\boldsymbol{k}} \sum_{\alpha\beta} \boldsymbol{\varepsilon} \cdot \hat{\boldsymbol{x}} \hat{P}_{\boldsymbol{k}\alpha} \hat{A}(\omega) \hat{P}_{\boldsymbol{k}\beta} \boldsymbol{\varepsilon} \cdot \hat{\boldsymbol{x}} \right).$$

Since $\mathbb{S}$ is an approximate symmetry, the off-diagonal blocks $\hat{P}_{\boldsymbol{k}\alpha} \hat{A} \hat{P}_{\boldsymbol{k}\beta}$ can be neglected. In addition, we can use the folding relations, Eq. (6), to replace the summation over the irreducible representation index α with the summation over the unfolded Brillouin zone to obtain

$$I(\omega) \sim \mathrm{tr}\left(\sum_{\boldsymbol{k}_{\alpha}} \boldsymbol{\varepsilon} \cdot \hat{\boldsymbol{x}} \hat{P}_{\boldsymbol{k}\alpha} \hat{A}(\omega) \hat{P}_{\boldsymbol{k}\alpha} \boldsymbol{\varepsilon} \cdot \hat{\boldsymbol{x}} \right), \qquad (13)$$

where $\boldsymbol{k}_{\alpha} = \boldsymbol{k} + \boldsymbol{k}_{f}^{\alpha\beta}, \forall \beta$, belong to the Brillouin zone unfolded in accordance with Eq. (6). In this case, the ARPES experiment will observe the spectral function $\hat{A}_{\boldsymbol{k}\alpha}(\omega) = \hat{P}_{\boldsymbol{k}\alpha} \hat{A}(\omega) \hat{P}_{\boldsymbol{k}\alpha}$ instead of the spectral function $\hat{A}_{\boldsymbol{k}}(\omega) = \hat{P}_{\boldsymbol{k}} \hat{A}(\omega) \hat{P}_{\boldsymbol{k}}$. One important detail in Eq. (13) is the fact that the irreducible representation α is only selected through the effect of dipole operators and the trace over the final states. This means that the actual irreducible representation observed in the experiment depends on the experimental conditions.

This is a very important conclusion, since it tells us that in order to carefully interpret raw ARPES data, we have to take into account two considerations. The first one is the possible effect of high-symmetry regions in the Brillouin zone. This implies the incorporation of point group operations into the unfolding—we would like to stress here that this issue is distinct from orbital symmetry selection by means of polarization. The second consideration is that we have to take into account all irreducible representations arising from the unfolding process and then use Eq. (6) to reconstruct the band structure from the ARPES data, if necessary.

Among the mentioned effects of high-symmetry regions of the Brillouin zone, the most important one is caused by the presence of the surface, which can effectively lower the dimensionality of states entering expression (12). This effect can be accounted for in our formalism by extending the two-dimensional restriction of the full translation group by
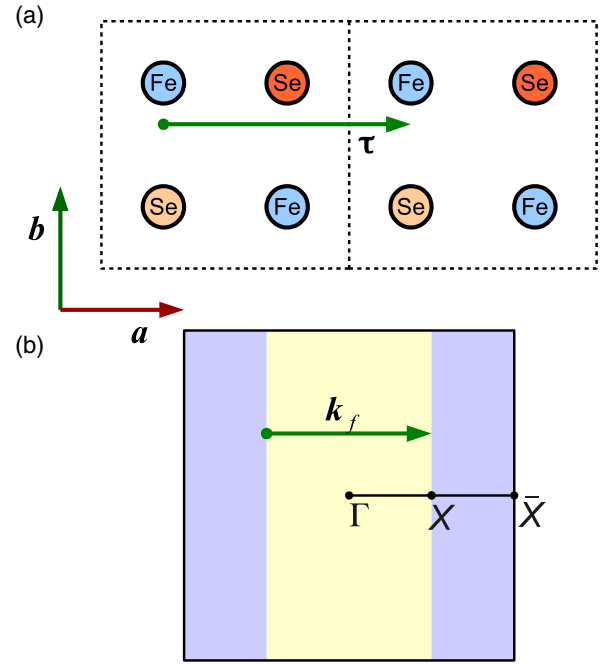

(a)

(b)

FIG. 2. (Color online) (a) Projection on the ab plane of a 2×1 supercell of tetragonal FeSe. The fractional translation $\boldsymbol{\tau}$ along $\boldsymbol{a}$ is shown in green. The iron atoms lie in the same plane, parallel to the plane of the drawing, while the lighter colored selenium atoms are vertically displaced above the plane, and the darker colored ones are below. (b) $k_z = 0$ plane of the Brillouin zone corresponding to the single unit cell of FeSe. The yellow filling marks the Brillouin zone corresponding to the supercell. The folding vector $\boldsymbol{k}_f$ is shown in green.

all point group operations that leave the surface invariant and then considering the resulting irreducible representations. We give an example of this by considering the application of the glide-reflection group to iron-based superconductors later on.

III. APPLICATIONS

Iron-based superconductors provide an excellent playground for the unfolding method presented here. The crystal structures of iron pnictides and iron chalcogenides consist of layers of Fe atoms tetrahedrally coordinated by the pnictogen/chalcogen atoms, as shown in Fig. 2(a). The various compounds may show differences in the stacking sequence of the iron pnictogen/chalcogen layers, as well as in the composition of the spacer layers. For most of the iron pnictide/chalcogenide families, a minimal translationally invariant unit cell consists of two iron and two pnictogen/chalcogen atoms. This unit cell can be reduced further by considering the glide-reflection operations, which combine the translations between the nearest-neighbor iron atoms with reflections in the xy plane, thus mapping two translationally inequivalent iron and pnictogen/chalcogen sites into each other.

In the following, we shall consider four representative unfolding examples. In the first case, we will apply translational unfolding on a 2×1 supercell of FeSe where the translational symmetry is kept in the supercell. In the second case, we will apply translational unfolding on a P-doped $CaFe_2As_2$ 2×2 supercell ($Ca_4Fe_8As_7P$), where the translational symmetry has
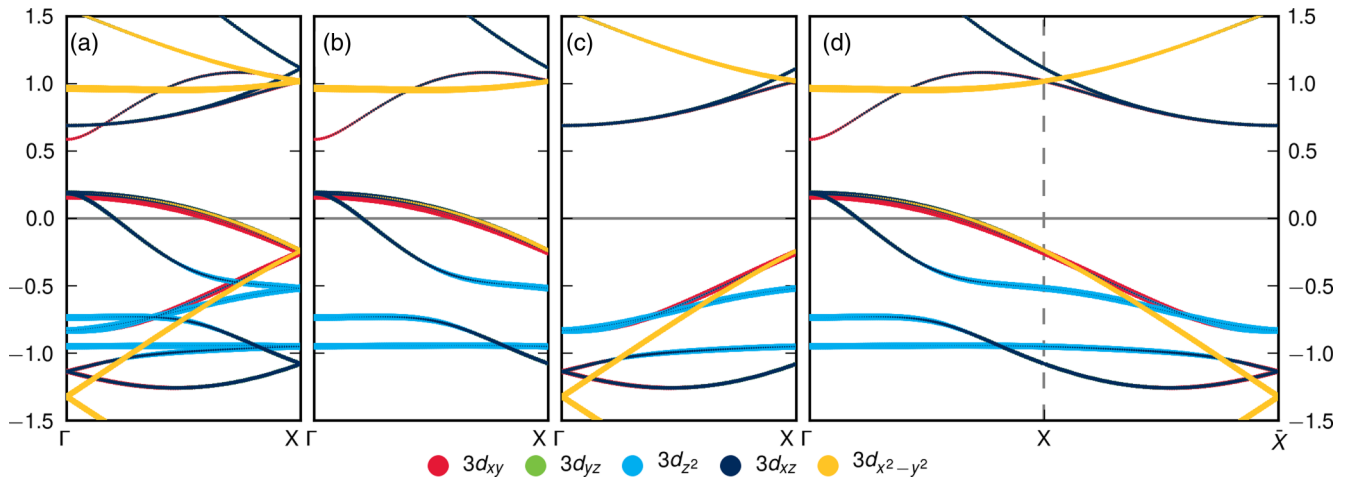
FIG. 3. (Color online) Unfolding of the tetragonal FeSe doubled along the $\boldsymbol{a}$ axis. (a) The folded band structure. (b) Projection of bands onto $\Delta^{(\boldsymbol{k},0)}$. (c) Projection of bands onto $\Delta^{(\boldsymbol{k},0)}$. (d) Unfolded picture. Irreducible representation $\Delta^{(\boldsymbol{k},0)}$ is extended past the boundaries of the Brillouin zone by the folding vector $\boldsymbol{k}_f = (\pi/a,0,0)$.

been broken by the substitution of one As by P. In the third case, we unfold the 16-band tight-binding model (2×5 Fe bands and 2×3 Se bands) for FeSe at 10 GPa to an 8-band tight-binding model. At this pressure, the structure shows important dispersion along k_z and it allows for an analysis of the unfolding procedure in all three directions. Finally, in the fourth case we apply unfolding of the two-iron unit cell to the one-iron unit cell representation in the specific case of the body-centered space group $I4/mmm$. With this last example, we want to show that the unfolding procedure is independent of whether the space group is body-centered or not.

A. Translational unfolding of FeSe

As a first example, we consider a simple case of translational unfolding, where the translation group $\mathbb{T}$ is expanded by fractional translations $\hat{C}_i = (1|\boldsymbol{\tau}_i)$. We define a 2×1 supercell of tetragonal FeSe [Fig. 2(a)] by doubling the unit cell along the $\boldsymbol{a}$ axis of FeSe. In Fig. 3(a), we show the corresponding supercell band structure along the path Γ-X [Fig. 2(b)]. To unfold the bands, we employ the fractional translation $\boldsymbol{\tau} = \boldsymbol{a}$, which is an additional symmetry that the supercell has on top of the translational symmetry $\mathbb{T}$. With this, the factor group $\mathbb{C}$ is isomorphic to the cyclic group of order 2, with the generator $(1|\boldsymbol{\tau})$, and from every irreducible representation $\mathbb{T}$, two irreducible representations with $\alpha = 0$ and 1 are induced, so that the generator Eq. (4) is represented by

$$\Delta^{(\boldsymbol{k},0)}((1|\boldsymbol{\tau})) = \exp(-i\boldsymbol{k} \cdot \boldsymbol{\tau}),$$
$$\Delta^{(\boldsymbol{k},1)}((1|\boldsymbol{\tau})) = -\exp(-i\boldsymbol{k} \cdot \boldsymbol{\tau}). \tag{14}$$

The resulting band projections onto the irreducible representations are shown in Figs. 3(b) and 3(c), while the unfolded picture, where the irreducible representation $\Delta^{(\boldsymbol{k},0)}$ is extended outside the supercell BZ, is shown in Fig. 3(d). Evidently, $\Delta^{(\boldsymbol{k}+\boldsymbol{k}_f,0)} = \Delta^{(\boldsymbol{k},1)}$, with $\boldsymbol{k}_f = (\pi/a,0,0)$.

B. Translational unfolding of P-doped CaFe$_2$As$_2$

The unfolding shown in Fig. 3 is perfect, because the fractional translation $(1|\boldsymbol{\tau})$ is an exact symmetry of the supercell

and every band will belong to only one of the irreducible representations of $\mathbb{S}$. In a more realistic case, where the operations $\hat{C}_i$ are only approximate symmetries, the bands will have nonzero projections onto multiple irreducible representations, although usually one of the irreducible representations will be dominantly present in every band. Such a situation occurs, for example, when studying doped compounds. Here we have chosen to investigate the phosphorus-doped CaFe$_2$As$_2$.

It is well known that when pressure is applied on CaFe$_2$As$_2$, it undergoes a magnetostructural phase transition from a magnetically ordered orthorhombic phase to a nonmagnetic, collapsed tetragonal phase [21,22]. In previous studies [23–25], we simulated the application of pressure under different conditions by means of density functional theory calculations, and we were able to predict the appearance of the collapsed tetragonal phase at a critical pressure that is accompanied by the disappearance of the Fermi surface pockets centered around the Γ point. This feature has been recently confirmed by angle-resolved photoemission experiments [26,27].

An orthorhombic to collapsed tetragonal phase transition in CaFe$_2$As$_2$ can also be induced by chemical pressure. For example, substitutional doping of phosphorus into the arsenic sites causes CaFe$_2$As$_2$ to enter the collapsed tetragonal phase at a doping level of around 5% [28]. To fully understand how chemical pressure is related to the application of physical pressure, we have performed a sequence of full structural relaxations of P-doped CaFe$_2$As$_2$. For the different doping levels, we have considered supercells of various sizes. Our density functional theory calculations predict that P-doped CaFe$_2$As$_2$ undergoes an orthorhombic to collapsed tetragonal phase transition for a doping between 9.375% and 12.5%, in good agreement with the experimental observations [28]. To analyze the electronic structure in the collapsed tetragonal phase of P-doped CaFe$_2$As$_2$, we have to perform the unfolding of the band structure.

Relaxed Ca(FeAs$_{0.875}$P$_{0.125}$)$_2$ has an orthorhombic unit cell where the phosphorus atom is breaking the translational symmetry, as shown in Fig. 4. The unit cell of Ca(FeAs$_{0.875}$P$_{0.125}$)$_2$ is a supercell consisting of four primitive unit cells of

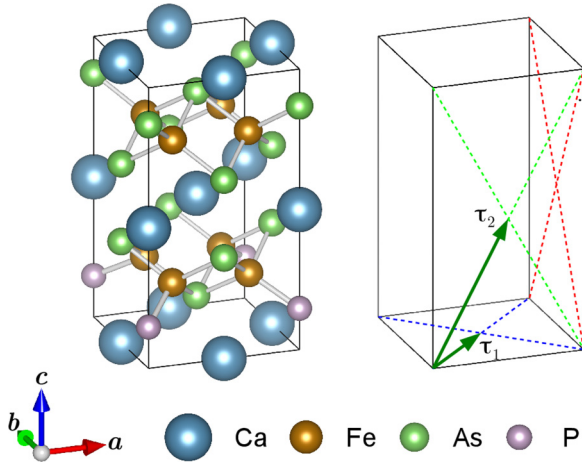FIG. 4. (Color online) The unit cell of $Ca(FeAs_{0.875}P_{0.125})_2$. The fractional translations $\boldsymbol{\tau}_i$ are shown in green.

$CaFe_2As_2$. This unit cell contains a total of eight iron atoms. The corresponding fractional translations are $\boldsymbol{\tau}_1 = (\boldsymbol{a} + \boldsymbol{b})/2$ and $\boldsymbol{\tau}_2 = (\boldsymbol{a} + \boldsymbol{c})/2$, where $\boldsymbol{a}$, $\boldsymbol{b}$, and $\boldsymbol{c}$ are the unit vectors of the supercell, as shown in Fig. 4. These fractional translations map the two translationally inequivalent iron atoms to the eight iron atoms of the supercell.

The corresponding band structure is shown in Fig. 5(a). The band structure is calculated along the path given by $(0,0,0) - (2\pi/a,0,0) - (2\pi/a,2\pi/a,0) - (0,0,0) - (0,0,2\pi/c)$. Four irreducible representations can be induced. We will select the irreducible representation $\Delta^{(\boldsymbol{k},0)}$ and extend it to the unfolded Brillouin zone. The resulting unfolded band structure, obtained by extending the irreducible representation $\Delta^{(\boldsymbol{k},0)}$, is shown in Fig. 5(b). Despite the fact that the fractional translations $\boldsymbol{\tau}_i$ are not the exact symmetries of $Ca(FeAs_{0.875}P_{0.125})_2$, the band projections onto different irreducible representations are still mostly orthogonal, having relatively clean unfolded bands as a result. This allows us to clearly see the disappearance of the hole pockets centered around Γ, since the set of three hole t_{2g} bands is pushed below the Fermi level by around 0.2 eV. Comparison of the unfolded bands to the band structure of the collapsed tetragonal phase of $CaFe_2As_2$ under pressure [24,26] confirms that phosphorus doping and application of hydrostatic

pressure affect the structural and electronic properties of $CaFe_2As_2$ in a remarkably similar way.

C. Unfolding from a 16-band to an 8-band tight-binding model for FeSe under pressure

We will now demonstrate the use of Eqs. (10) and (11) for the unfolding of tight-binding models. We consider as a test system FeSe at 10 GPa with significant dispersion in all three directions. The crystal structure has been obtained from *ab initio* simulations of hydrostatic pressure at 10 GPa [24,25]. We have used the projective Wannier functions as implemented in the FPLO code [29] for the derivation of the 16-band tight-binding model, which consists of five $3d$ orbitals per iron site and three $4p$ orbitals per selenium site. The structure under 10 GPa of hydrostatic compression is chosen because the three-dimensional character of the Fermi surface is more pronounced compared to ambient pressure.

As previously mentioned, the two translationally nonequivalent iron sites can be mapped onto each other with the help of the glide-reflection operations $\hat{C}_i = (\boldsymbol{\tau}_i|\hat{\sigma}_z)$ with $i = 1,2$. The fractional translations $\boldsymbol{\tau}_i$ connect the nearest-neighbor iron atoms as shown in Fig. 2(a), while $\hat{\sigma}_z$ is a reflection in the xy plane. To unfold, we can choose one of the $\hat{C}_i$ operations and then induce the irreducible representations of $\mathbb{S} = \mathbb{T} \cup \mathbb{T}\hat{C}_i$. In accordance with Ref. [12], we call $\mathbb{S}$ the glide-reflection group. Since the factor group is of index 2, two one-dimensional irreducible representations will be induced in the $k_z = 0$ plane of the Brillouin zone. Because the electronic dispersion in FeSe is weaker along the $\boldsymbol{k}_z$ axis, we can expect that irreducible representations induced in the $k_z = 0$ plane will give adequate unfolding across the rest of the Brillouin zone.

In these two irreducible representations, the glide-reflection operation will have the same representation as did the fractional translation in Eq. (14). However, what differentiates the case of the glide-reflection unfolding from the purely translational unfolding is the orbitally selective action of the matrices $\hat{W}(\hat{C}_i)$ in Eq. (7). Namely, in the case of translational unfolding, matrices $\hat{W}(\hat{C}_i)$ act equally on all orbitals, while in the case of glide-reflection unfolding they act differently, depending on whether the orbitals are symmetric or antisymmetric with respect to the reflections in the xy plane.
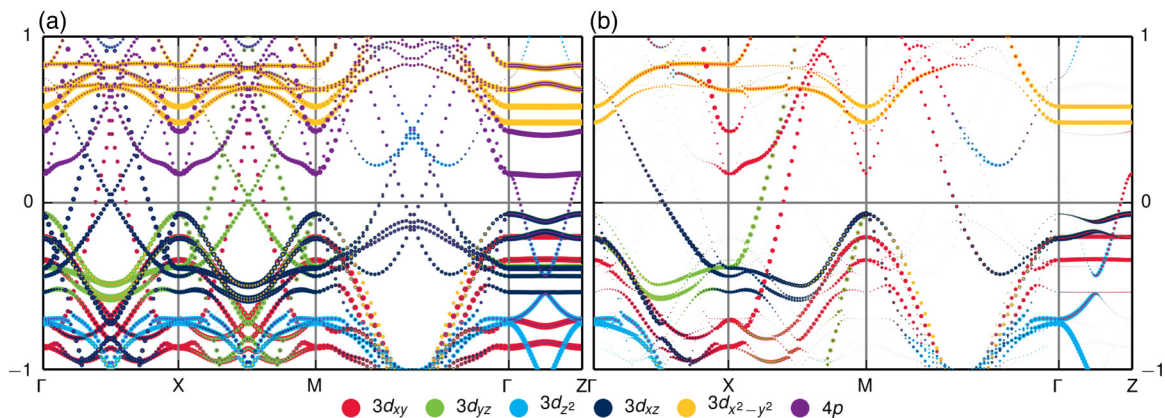

FIG. 5. (Color online) Unfolding of $Ca(FeAs_{0.875}P_{0.125})_2$ band structure. (a) Band structure of the $Ca(FeAs_{0.875}P_{0.125})_2$ supercell. (b) The unfolded band structure obtained from $\Delta^{(\boldsymbol{k},0)}$.
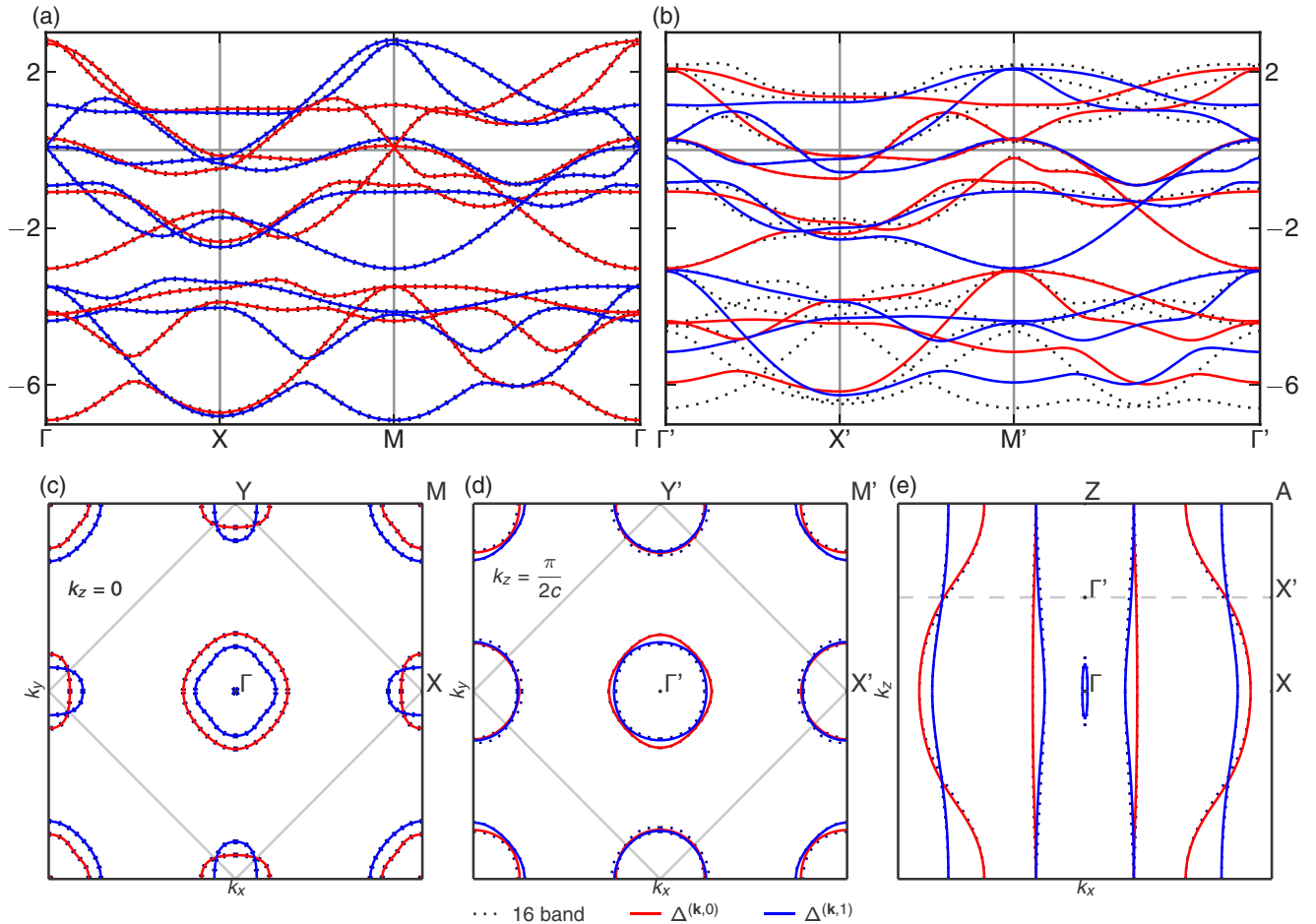
FIG. 6. (Color online) Unfolding of the 16-band tight-binding model of FeSe with the help of glide-reflection operations. The 16-band result is shown with dots, the two 8-band results with lines. (a) Band structure along the path in the $k_z = 0$ plane of the one-iron equivalent Brillouin zone. (b) Band structure along the path parallel to the path shown in (a), but shifted along the $\boldsymbol{k}_z$ axis by $\pi/2c$. (c) Fermi surface cut at the $k_z = 0$ plane of the one-iron equivalent Brillouin zone of FeSe. The solid gray line shows the boundary of the two-iron Brillouin zone. (d) Fermi surface cut at the $k_z = \pi/2c$ plane of the one-iron equivalent Brillouin zone of FeSe. (e) Fermi surface cut at the $k_y = 0$ plane of the one-iron equivalent Brillouin zone of FeSe. The dashed gray line shows the location of $k_z = \pi/2c$.

For example, the $3d_{z^2}$ orbital will stay invariant, while $3d_{xz}$ will pick up a minus sign under the action of $\hat{\sigma}_z$.

We have used Eq. (10) to create the two sets of hopping energies, corresponding to two induced irreducible representations. These two sets correspond to the same 8-band tight-binding model, up to the unitary transformation. The band structure calculated from the 16-band and two 8-band tight-binding models along the path in the $k_z = 0$ plane of the Brillouin zone is shown in Fig. 6(a). The corresponding Fermi surface slice in the $k_z = 0$ plane is shown in Fig. 6(c). In accordance with Eq. (6) and the electronic structure shown in Fig. 6, the folding vector is $\boldsymbol{k}_f^{01} = (\pi,\pi,0)$ with respect to the one-iron Brillouin zone (as a convention, we will always specify folding vectors with respect to the unfolded Brillouin zone). It is evident that the unfolding to the 8-band model is perfect in the $k_z = 0$ plane. Since the $k_z = \pm\pi/c$ planes are also the high-symmetry planes for the reflections in the xy plane, the unfolding will be perfect there, too. We can thus expect the largest deviations from the perfect unfolding around the $k_z = \pm\pi/2c$ plane. This can be seen in the band structure shown in Fig. 6(b), taken along the path shown in Fig. 6(a) shifted by $(0,0,\pi/2c)$. The

deviations of the unfolded bands are evident. However, the deviations of the top ten bands, which are the bands dominated by the $3d$ orbital character, are much smaller than in the bands dominated by the $4p$ orbital character. This is a consequence of the crystal structure; the iron atoms are stationary under the action of $\hat{\sigma}_z$, while the selenium atoms are not. Due to this property, the Fermi surface can be unfolded almost exactly across the entire Brillouin zone. The Fermi surface slice in the $k_z = \pi/2c$ is shown in Fig. 6(d), while the vertical slice in the $k_y = 0$ plane is shown in Fig. 6(e). It is remarkable that the full three-dimensional structure of the innermost Fermi surface pocket, centered at Γ, is retained with high accuracy in the unfolded model, despite the fact that the underlying unfolding symmetry is purely two-dimensional.

D. Unfolding the band structure of CaFe$_2$As$_2$ to the one-iron equivalent Brillouin zone

Finally, we would like to point out that the glide-reflection group can also be used to unfold the band structures of iron-based superconductors with a centered unit cell, described
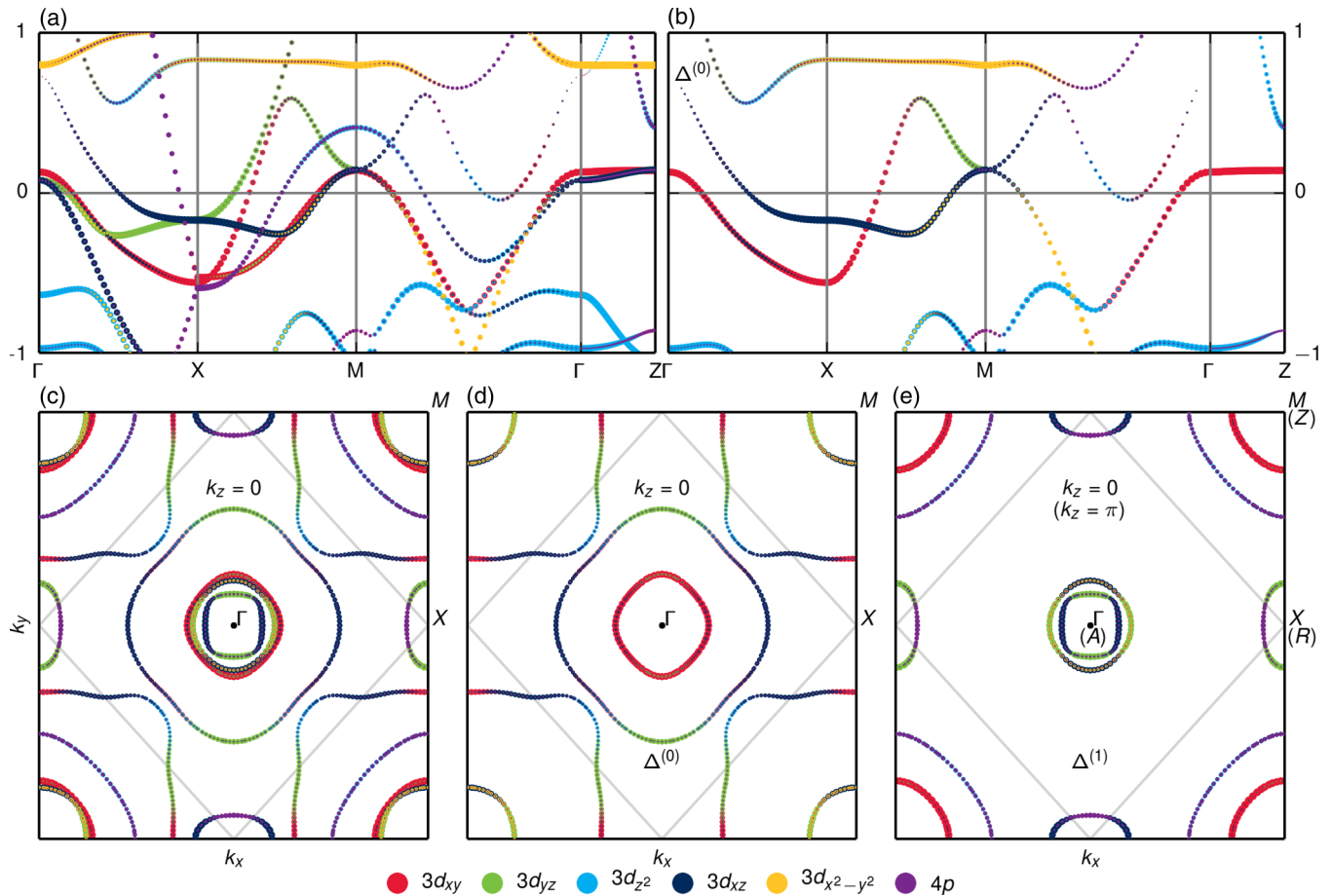
FIG. 7. (Color online) Unfolding of $CaFe_2As_2$ band structure to the one-iron equivalent Brillouin zone. (a) Band structure of $CaFe_2As_2$ in the two-iron Brillouin zone. (b) The unfolded band structure obtained from $\Delta^{(k,0)}$ in the one-iron equivalent Brillouin zone. (c) $k_z = 0$ cut of the $CaFe_2As_2$ Fermi surface cut in the two-iron Brillouin zone. (d) and (e) Projection of the Fermi surface obtained from $\Delta^{(k,0)}$ and $\Delta^{(k,1)}$, respectively. Labels enclosed in brackets in panel (e) pertain to the $k_z = \pi$ cut of the Fermi surface.

by symmorphic space groups. In this particular example, we use the ambient pressure structure of $CaFe_2As_2$ measured at a temperature $T = 250$ K and described by the body-centered space group $I4/mmm$ [22]. $CaFe_2As_2$ was selected because it features additional electron Fermi surface pockets that make the one-iron Fermi surface determination more complicated.

The glide-reflection operations as well as the irreducible representations are identical to the case of FeSe. The main difference here is that the resulting folding vector is (π,π,π), corresponding to the unfolding onto the simple tetragonal one-iron unit cell. This result is not immediately obvious, since we are only using the symmetry of the iron-arsenic layer, and it is to be expected, in the naive picture, that the resulting unfolding would result in the one-iron body-centered unit cell and the $(\pi,\pi,0)$ folding vector. However, due to the body-centered symmetry, the $(\pi,\pi,0)$ folding vector relates Γ and Z points, as shown in Fig. 8. In addition, unlike (π,π,π), the $(\pi,\pi,0)$ folding vector does not satisfy the folding relations, Eq. (6), which is a nice example underlining their usefulness.

Figure 7(a) shows the band structure in the two-iron equivalent Brillouin zone, while Fig. 7(b) shows the unfolded band structure in the one-iron equivalent Brillouin zone obtained by extending $\Delta^{(k,0)}$. Evidently, the unfolding remains

perfect in the $k_z = 0$ plane. However, this is no longer the case across the entire Brillouin zone. For instance, along the Γ-Z path, weak traces of bands from $\Delta^{(k,1)}$ can be observed.
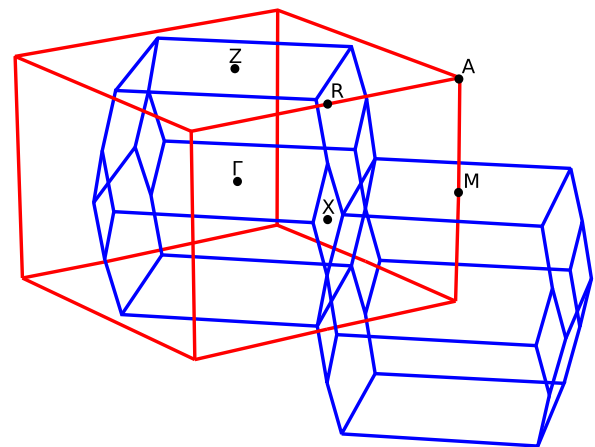

FIG. 8. (Color online) One- and two-iron Brillouin zones for the $I4/mmm$ space group. Two adjacent Brillouin zones corresponding to the two-iron primitive cell of the $I4/mmm$ space group are shown in blue. The simple tetragonal unit cell corresponding to the one-iron unit cell is shown in red.

In comparison to FeSe, in the vicinity of the Fermi level, the CaFe$_2$As$_2$ band structure features more orbital weight of arsenic $4p$ and some calcium $3d$ character, which makes unfolding outside of the high-symmetry plane less accurate. Nevertheless, we have enough information to clearly discern the topology of the unfolded Fermi surface. Figures 7(c)–7(e) show the $k_z = 0$ cut of the CaFe$_2$As$_2$ Fermi surface. Because of the body-centered arrangement of the Brillouin zones shown in Fig. 8, this is also the $k_z = \pi$ cut of the Fermi surface, offset by $(\pi,\pi,0)$, and as a result the connectivity of the Fermi surface elements can be deduced between the $k_z = 0$ and $k_z = \pi$ planes.

IV. DISCUSSION

A. One-iron versus two-iron picture

The above results have important implications for the one-iron versus two-iron discussion in the iron pnictide literature [13]. Since simulations of some processes, such as multiorbital pairing, scale as the sixth power [30] of the number of orbitals involved, it is important to keep the models as simple as possible. In addition, careful consideration of symmetry has very important consequences for the superconducting state [31–33]. For this reason, one needs to understand the exact conditions and the symmetry context in which the one-iron model can be used.

When the unfolding is considered as a projection onto the irreducible subspace of the glide-reflection group, some potentially important subtleties arise in comparison to the conclusions drawn in Ref. [13]. As long as the electronic structure in the energy range of interest is dominated by the iron orbitals and all dynamics under consideration involve at least approximate glide-reflection symmetry, a one-iron tight-binding model can be used without significant impact on the overall accuracy of the calculation. Furthermore, even in the cases in which the glide-reflection symmetry is not so favorable, a controlled one-iron approximation can be made since the off-diagonal blocks in the decomposition onto irreducible subspaces can provide an error estimate. In addition, this shows that only the glide-reflection group can provide criteria that unambiguously resolve Fermi surface elements in the process of unfolding to the one-iron Brillouin zone.

Furthermore, our discussion of the effects of high-symmetry regions of the Brillouin zone on the interpretation of ARPES data shows that under certain conditions it is possible to observe the spectral function consistent with the one-iron picture in the $k_z = 0$ or $k_z = \pi$ planes. This is corroborated by recent observations [34] in CsFe$_2$As$_2$, whose electronic structure is weakly dispersive in the k_z direction, and the glide-reflection unfolding can be accurately extended across the entire Brillouin zone.

The unfolding process also offers a simple answer to the question of why the neutron scattering intensities seem to indicate a scenario consistent with the one-iron picture [35,36]. This can be naturally interpreted as a consequence of the fact that neutron scattering intensities are momentum-resolved in the high-symmetry plane, and transitions between states belonging to different irreducible subspaces are suppressed there.

V. SUMMARY

In summary, we have demonstrated with a group-theoretical treatment of the band structure that unfolding can be understood as a projection onto induced irreducible representations of the supergroup of the original translation group. The unfolded Brillouin zone arises as a consequence of the fact that different induced irreducible representations become identical when shifted by an appropriate vector in the Brillouin zone. Due to the projective definition, the unfolding procedure can be generalized for arbitrary quantities in reciprocal space. Also, the unfolding artifacts in the cases in which the unfolding is inexact arise because bands have nonzero projections onto multiple irreducible representations.

When point group operations are used, the unfolding is exact only in the high-symmetry k points of the Brillouin zone. It is nonetheless possible to extend the unfolding to the entire Brillouin zone as long as the band structure is dominantly dispersive only along the corresponding high-symmetry lines or planes in the Brillouin zone. By making sure this constraint is satisfied, it is possible to formulate tight-binding models of reduced dimensionality without loss of accuracy. In the cases in which this is not completely possible, the unfolding framework provides a systematic way to make controlled approximations by projecting the relevant quantities into appropriate irreducible subspaces.

For FeSe under pressure, we have shown how an 8-band tight-binding model can be constructed by unfolding the 16-band tight-binding model with the help of glide-reflection operations. The resulting unfolded model produces the almost exactly unfolded Fermi surface. This results from the fact that the Fermi surface in FeSe is dominated by the iron orbital character. This is in fact the most important requirement that needs to be fulfilled for the one-iron model to be an accurate representation of the physics of iron-based superconductors. An additional requirement stems from the fact that the one-iron picture is formulated as an irreducible representation, and as such for any realistic computation using the one-iron model, the off-diagonal elements of the involved observables connecting the two irreducible representations of the glide-reflection group need to be small compared to the diagonal elements.

And finally, we show that careful interpretation of ARPES data in cases in which a direct comparison with density functional theory calculations is not immediately obvious requires consideration of possible effects of high-symmetry regions of the Brillouin zone as well as comparison with all irreducible representations arising from the unfolding process. An implementation of the translational unfolding procedure for the VASP code is available online [37].

[1] P. Hohenberg and W. Kohn, Phys. Rev. **136**, B864 (1964).
[2] F. Bloch, Z. Phys. **52**, 555 (1929).
[3] T. B. Boykin and G. Klimeck, Phys. Rev. B **71**, 115215 (2005).
[4] T. B. Boykin, N. Kharche, and G. Klimeck, Phys. Rev. B **76**, 035310 (2007).
[5] T. B. Boykin, N. Kharche, G. Klimeck, and M. Korkusinski, J. Phys. Condens. Matter **19**, 036203 (2007).
[6] W. Ku, T. Berlijn, and C.-C. Lee, Phys. Rev. Lett. **104**, 216401 (2010).
[7] V. Popescu and A. Zunger, Phys. Rev. B **85**, 085201 (2012).
[8] P. V. C. Medeiros, S. Stafström, and J. Björk, Phys. Rev. B **89**, 041407(R) (2014).
[9] H. Huang, F. Zheng, P. Zhang, J. Wu, B.-L. Gu, and W. Duan, New J. Phys. **16**, 033034 (2014).
[10] M. X. Chen and M. Weinert, Nano Lett. **14**, 5189 (2014).
[11] E. P. Wigner, *Gruppentheorie und ihre Anwendung auf die Quantenmechanik der Atomspektren* (Vieweg, Wiesbaden, 1931).
[12] O. K. Andersen and L. Boeri, Ann. Phys. (NY) **523**, 8 (2011).
[13] C.-H. Lin, T. Berlijn, L. Wang, C.-C. Lee, W.-G. Yin, and W. Ku, Phys. Rev. Lett. **107**, 257001 (2011).
[14] M. El-Batanouny and F. Wooten, *Symmetry and Condensed Matter Physics; A Computational Approach* (Cambridge University Press, New York, 2008).
[15] S. K. Kim, *Group Theoretical Methods and Applications to Molecules and Crystals* (Cambridge University Press, Cambridge, 1999).
[16] G. Kresse and J. Hafner, Phys. Rev. B **47**, 558 (1993).
[17] A. Damascelli, Phys. Scr. **T109**, 61 (2004).
[18] S.-H. Lee, G. Xu, W. Ku, J. S. Wen, C. C. Lee, N. Katayama, Z. J. Xu, S. Ji, Z. W. Lin, G. D. Gu, H.-B. Yang, P. D. Johnson, Z.-H. Pan, T. Valla, M. Fujita, T. J. Sato, S. Chang, K. Yamada, and J. M. Tranquada, Phys. Rev. B **81**, 220502(R) (2010).
[19] G. Borstel, Appl. Phys. A **38**, 193 (1985).
[20] W. Nolting, J. Braun, G. Borstel, and W. Borgiel, Phys. Scr. **41**, 601 (1990).
[21] M. S. Torikachvili, S. L. Budko, N. Ni, and P. C. Canfield, Phys. Rev. Lett. **101**, 057006 (2008).
[22] A. Kreyssig, M. A. Green, Y. Lee, G. D. Samolyuk, P. Zajdel, J. W. Lynn, S. L. Bud'ko, M. S. Torikachvili, N. Ni, S. Nandi, J. B. Leão, S. J. Poulton, D. N. Argyriou, B. N. Harmon, R. J. McQueeney, P. C. Canfield, and A. I. Goldman, Phys. Rev. B **78**, 184517 (2008).
[23] Y-Z. Zhang, H. C. Kandpal, I. Opahle, H. O. Jeschke, and R. Valentí, Phys. Rev. B **80**, 094530 (2009).
[24] M. Tomić, R. Valentí, and H. O. Jeschke, Phys. Rev. B **85**, 094105 (2012).
[25] M. Tomić, H. O. Jeschke, R. M. Fernandes, and R. Valentí, Phys. Rev. B **87**, 174503 (2013).
[26] R. S. Dhaka, R. Jiang, S. Ran, S. L. Bud'ko, P. C. Canfield, B. N. Harmon, A. Kaminski, M. Tomić, R. Valentí, and Y. Lee, Phys. Rev. B **89**, 020511(R) (2014).
[27] K. Gofryk, B. Saparov, T. Durakiewicz, A. Chikina, S. Danzenbächer, D. V. Vyalikh, M. J. Graf, and A. S. Sefat, Phys. Rev. Lett. **112**, 186401 (2014).
[28] S. Kasahara, T. Shibauchi, K. Hashimoto, Y. Nakai, H. Ikeda, T. Terashima, and Y. Matsuda, Phys. Rev. B **83**, 060505(R) (2011).
[29] K. Koepernik and H. Eschrig, Phys. Rev. B **59**, 1743 (1999).
[30] S. Graser, T. A. Maier, P. J. Hirschfeld, and D. J. Scalapino, New J. Phys. **11**, 025016 (2009).
[31] V. Cvetković and O. Vafek, Phys. Rev. B **88**, 134510 (2013).
[32] M. Casula and S. Sorella, Phys. Rev. B **88**, 155125 (2013).
[33] C.-H. Lin, C.-P. Chou, W.-G. Yin, and W. Ku, arXiv:1403.3687.
[34] S. Kong, D. Y. Liu, S. T. Cui, S. L. Ju, A. F. Wang, X. G. Luo, L. J. Zou, X. H. Chen, G. B. Zhang, and Z. Sun, arXiv:1409.2300.
[35] M. D. Lumsden, A. D. Christianson, E. A. Goremychkin, S. E. Nagler, H. A. Mook, M. B. Stone, D. L. Abernathy, T. Guidi, G. J. MacDougall, C. de la Cruz, A. S. Sefat, M. A. McGuire, B. C. Sales, and D. Mandrus, Nat. Phys. **6**, 182 (2010).
[36] J. T. Park, D. S. Inosov, A. Yaresko, S. Graser, D. L. Sun, Ph. Bourges, Y. Sidis, Y. Li, J.-H. Kim, D. Haug, A. Ivanov, K. Hradil, A. Schneidewind, P. Link, E. Faulhaber, I. Glavatskyy, C. T. Lin, B. Keimer, and V. Hinkov, Phys. Rev. B **82**, 134503 (2010).
[37] http://github.com/tomkeus/vasp_unfold.